Available online at www.sciencedirect.com
SCIENCE DIRECT®
Nuclear Instruments and Methods in Physics Research A 545 (2005) 309–318
NUCLEAR INSTRUMENTS & METHODS IN PHYSICS RESEARCH Section A
www.elsevier.com/locate/nima

Cold and thermal neutron scattering in liquid water—II: Scattering laws and group constants for H_2O and D_2O

Yoshinobu Edura*, Nobuhiro Morishima

Department of Nuclear Engineering, Kyoto University, Yoshida-Honmachi, Sakyo-ku, Kyoto 606-8501, Japan

Received 16 December 2004; accepted 10 January 2005
Available online 11 March 2005

Abstract

On the basis of the cross-section model of liquid H_2O, which has been developed in the previous paper, cold and thermal neutron scattering in liquid D_2O is described. The dynamics of liquid molecules, together with their static distribution, is fully taken into account so that various results of neutron experiments and computer simulations are well reproduced especially in terms of coherent scattering like the diffuse Bragg one. The model covers a wide range of neutron incident energies from 0.1 μeV to 10 eV at many different temperatures between 0 and 100 °C. Double-differential and total scattering cross sections are calculated by the use of a generalized frequency distribution and, equivalently, a velocity auto-correlation function. Furthermore, a set of scattering laws and group constants for liquid H_2O and D_2O is generated, which will be useful for research and development of an advanced neutron source and a nuclear power reactor.

PACS: 61.25.Em; 78.70.Nx; 28.20.Gd; 29.25.Dz

Keywords: Light water; Heavy water; Neutron cross section; Cold neutron source; Scattering law; Group constant

1. Introduction

In the previous paper [1], the cross-section model for incoherent inelastic neutron scattering in light water (H_2O) has been developed. It is expressed as a dynamics model of a single water molecule in terms of a generalized frequency distribution (GFD) and, equivalently, a velocity auto-correlation function (VACF) in a time scale ranging from 0.1 fs to 1 μs. Inherent molecular motions in liquid H_2O are described by the jump diffusion and intermolecular vibration due to the hydrogen-bond network, together with hindered rotation and intramolecular vibration. The double-differential and total scattering cross sections for incident neutron energies of 0.1 μeV (ultra-cold)–10 eV (epi-thermal) are calculated. The results show satisfactory agreement with the neutron scattering experiments and computer simulations at many different temperatures [2–11].

*Corresponding author. Tel./fax: +81 75 753 5836.
E-mail address: edura@nucleng.kyoto-u.ac.jp (Y. Edura).

0168-9002/$ - see front matter © 2005 Elsevier B.V. All rights reserved.
doi:10.1016/j.nima.2005.01.302

The present paper generalizes the cross section model of liquid H_2O to the one of liquid D_2O. Coherent neutron scattering is treated in view of a microscopic static structure and molecular motions. The dynamics of a D_2O molecule is described in the same framework with the one of H_2O and determined using various model parameters through physical consideration and by comparison with the results of neutron experiments and computer simulations [5,6,12]. The coherent scattering is simply expressed in the Vineyard approximation [13] because of a wide range of cross-section calculation for neutron energy and liquid temperature. A set of partial static structure factors (PSSFs) $S^X(Q)$ for pairs of $X = \mathrm{DD}$, DO, OO, determined experimentally [14], is utilized for description of interference scattering from distinct molecules. The resultant cross-section model is in contrast with such earlier ones as Nelkin model and Honeck model [15,16] that represent molecular translation by a free-gas model, though they have been employed for

Table 1
Physical constants and parameters for the present D_2O model

Definition	Symbol (Unit)	D	O
Atomic mass	M (meV ps^2 Å^{-2})	0.2090	1.658
Bound-atom coherent scattering length	b_{coh} (fm)	6.672	5.804
Bound-atom incoherent scattering length	b_{inc} (fm)	4.023	0.000
Absorption cross section	σ_{a} (b atom^{-1}) at 25 meV	0.000519	0.000
Translational diffusion (d)			
Diffusion coefficient	$D_{\mathrm{t}}^{\mathrm{D_2O}}(T)$ (Å^2 ps^{-1})	$258.2 \times \exp(-2.108\,\frac{1000}{T})/1.28$	
Residence time	$\tau_0^{\mathrm{D_2O}}(T)$ (ps) $(= \tau_0^{\mathrm{H_2O}}(T))$	$1.548 \times 10^{-4} \times \exp(2.648\,\frac{1000}{T})$	
Effective mass	$M_{\mathrm{d}}^{\mathrm{D_2O}}(T)$ (meV ps^2 Å^{-2})	$\tau_0^{\mathrm{D_2O}}(T) k_{\mathrm{B}} T / D_{\mathrm{t}}^{\mathrm{D_2O}}(T)$	
Intermolecular vibration (t)			
Bending mode	$\varepsilon_{\mathrm{t}1}^{\mathrm{D}0}$ at 20 °C $(= \varepsilon_{\mathrm{t}1}^{\mathrm{H}0})$	0.016	
	$\varepsilon_{\mathrm{t}1}(T)$, $\hbar\omega_{\mathrm{t}1}^{\mathrm{D_2O}}$ (meV)	Eq. (55) in Ref. [1], Eq. (7)	Eq. (57) in Ref. [1], Eq. (7)
Stretching mode	$\varepsilon_{\mathrm{t}2}^{\mathrm{D}0}$ at 20 °C $(= \varepsilon_{\mathrm{t}2}^{\mathrm{H}0})$	0.028	
	$\varepsilon_{\mathrm{t}2}(T)$, $\hbar\omega_{\mathrm{t}2}^{\mathrm{D_2O}}$ (meV)	Eq. (55) in Ref. [1], Eq. (7)	Eq. (57) in Ref. [1], Eq. (7)
Rotational diffusion (RD)			
Rotational diffusion coefficient	$D_{\mathrm{r}}^{\mathrm{D_2O}}(T)$ (ps^{-1})	$[6\tau_{\mathrm{RD}}^{\mathrm{D_2O}}(T)]^{-1}$	—
Rotational relaxation time	$\tau_{\mathrm{RD}}^{\mathrm{D_2O}}(T)$ (ps) $(= \tau_{\mathrm{RD}}^{\mathrm{H_2O}}(T))$	$0.0485 \times \exp(80.7/k_{\mathrm{B}}T)$	—
Bond length of D–O	R (Å)	0.91	—
Mass ratio	$M^{\mathrm{D}}/M_{\mathrm{r}}^{\mathrm{D}}$ $(= M^{\mathrm{H}}/M_{\mathrm{r}}^{\mathrm{H}})$	0.0006	—
Hindered rotation (HR)	$\varepsilon_{\mathrm{HR}}^{\mathrm{D}0}$ at 20 °C $(= \varepsilon_{\mathrm{HR}}^{\mathrm{H}0})$	0.5548	
	$\varepsilon_{\mathrm{HR}}^{\mathrm{D}}(T)$, $\hbar\omega_{\mathrm{HR}}^{\mathrm{D_2O}}$ (meV)	Eq. (56) in Ref. [1], Eq. (8)	—
Intramolecular vibration (v)			
Bending mode	$\varepsilon_{\mathrm{v}1}$, $\hbar\omega_{\mathrm{v}1}^{\mathrm{D_2O}}$ (meV), $\sigma_{\mathrm{v}1}$ (meV)	0.133, Eq. (8), 5.0	0.0233, Eq. (8), 5.0
Stretching mode	$\varepsilon_{\mathrm{v}2}$, $\hbar\omega_{\mathrm{v}2}^{\mathrm{D_2O}}$ (meV), $\sigma_{\mathrm{v}2}$ (meV)	0.133, Eq. (8), 10.0	0.0233, Eq. (8), 10.0
Asymmetric-stretching mode	$\varepsilon_{\mathrm{v}3}$, $\hbar\omega_{\mathrm{v}3}^{\mathrm{D_2O}}$ (meV), $\sigma_{\mathrm{v}3}$(meV)	0.133, Eq. (8), 10.0	0.0233, Eq. (8), 10.0

$m = 0.1045\,\mathrm{meV\,ps^2\,Å^{-2}}$, $\hbar = 0.6582\,\mathrm{meV\,ps}$ and $k_{\mathrm{B}} = 0.08617\,\mathrm{meV\,K^{-1}}$.

generation of the widespread thermal neutron scattering library ENDF/B-IV [17,18]. We have newly constructed two cross section libraries in different format, group constants (energy-averaged cross sections) and scattering laws. The former may be commonly used in a multi-group neutron transport analysis and the latter in a continuous-energy Monte Carlo calculation. By a combination with the already-generated libraries for liquid H_2 and D_2 and solid CH_4 [19–22], we may proceed to study design and analysis of an advanced cold-neutron source [23–25].

The present paper is organized as follows. Section 2 describes the double-differential scattering cross-section (DDX) model for cold and thermal neutron scattering in liquid D_2O. Section 3 demonstrates quantitative comparison with the neutron experiments [5,6] and the computer simulations [12] in terms of the GFD and the DDX. Section 4 presents the scattering laws and the group constants of liquid H_2O and D_2O. Section 5 is devoted to the concluding remarks. All the parameter values of the model for liquid D_2O are listed in Table 1.

2. Cross-section model

The DDX for liquid D_2O may be defined using the self-scattering functions (SSFs) $S_s^D(Q,\omega)$ and $S_s^O(Q,\omega)$ by the Vineyard's convolution approximation [13]:

$$\left(\frac{d^2\sigma}{d\Omega\, dE'}\right)^{D_2O} = 2\frac{k'}{k}{b_{coh}^D}^2\left\{1+2\gamma^{DD}(Q)+\frac{b_{coh}^O}{b_{coh}^D}\gamma^{DO}(Q)\right\}S_s^D(Q,\omega)+\frac{k'}{k}{b_{coh}^O}^2\times\left\{1+\gamma^{OO}(Q)+2\frac{b_{coh}^D}{b_{coh}^O}\gamma^{DO}(Q)\right\}S_s^O(Q,\omega)+2\frac{k'}{k}{b_{inc}^D}^2S_s^D(Q,\omega)+\frac{k'}{k}{b_{inc}^O}^2S_s^O(Q,\omega) \quad (1)$$

where the PSSFs $S^X(Q)$ $(X = DD, DO, OO)$ are expressed as

$$\gamma^{DD}(Q) = S^{DD}(Q) - 1, \quad \gamma^{DO}(Q) = S^{DO}(Q) - 1, \quad \gamma^{OO}(Q) = S^{OO}(Q) - 1. \quad (2)$$

k and k' are the wave numbers for incident and scattered neutrons, respectively, b_{coh}^D and b_{coh}^O are the bound-atom coherent scattering lengths, b_{inc}^D and b_{inc}^O are the bound-atom incoherent scattering lengths, Q and ω are the momentum and energy transfers defined as

$$\hbar\vec{Q} = \hbar\vec{k}' - \hbar\vec{k} \quad (3)$$

$$\hbar\omega = E' - E \quad (4)$$

with the Planck's constant $\hbar$ and E and E' are the incident and scattered neutrons energies, respectively. Supposing that all $\gamma^X(Q) = 0$, Eq. (1) leads to the DDX by incoherent approximation [1]. Note that $\omega > 0$ and $\omega < 0$ indicate energy-gain (up) and energy-loss (down) scattering, respectively.

Eq. (1) describes coherent scattering in liquid D_2O in terms of the product of the PSSF and SSF. The former relates to the interference effect of neutron scattering by distinct molecules and the latter represents the motion of an individual molecule. Hence the collective excitations of molecules propagated through a hydrogen-bonds network like phonon is out of consideration, though they have been observed by inelastic neutron scattering on the dispersion curve of phonon [26,27]. The PSSFs $S^X(Q)$ are taken from the experimental results estimated by the combination of X-ray, electron and neutron diffractions [14].

Since the SSF model for liquid H_2O has been developed in the previous work [1], we apply it to liquid D_2O. The values of model parameters are selected properly by the following physical considerations.

- The diffusion coefficient $D_t^{D_2O}(T)$ is assumed to obey an Arrhenius behavior like liquid H_2O and have a magnitude determined by the fitting of the experimental results [28–30]:

$$D_t^{D_2O}(T) = D_t^{H_2O}(T)/1.28 \quad (5)$$

where

$$D_t^{H_2O}(T) = 258.2 \times \exp\left(-2.108\frac{1000}{T}\right)(\text{Å}^2\,\text{ps}^{-1}) \quad (6)$$

and T is the absolute temperature of liquid D_2O in K.

- We identify a residence time $\tau_0^{D_2O}(T)$ in the translational diffusion and a rotational relaxation time $\tau_{RD}^{D_2O}(T)$ in the rotational diffusion with the corresponding ones for liquid H_2O, $\tau_0^{H_2O}(T)$ and $\tau_{RD}^{H_2O}(T)$, respectively.
- Characteristic frequencies $\omega_{t\,m}^{D_2O}$ $(m = 1, 2)$ of the intermolecular vibrations (bending and stretching modes) may be determined from the corresponding ones $\omega_{t\,m}^{H_2O}$ by taking account of the molecular mass difference between H_2O and D_2O:

$$\omega_{t\,m}^{D_2O} = \sqrt{\frac{18}{20}}\omega_{t\,m}^{H_2O}. \tag{7}$$

- The hindered rotation of a molecule and the intramolecular vibrations (bending, stretching and asymmetric stretching modes) are assumed to take place around the center of mass very near the position of O. Hence, their characteristic frequencies $\omega_{HR}^{D_2O}$ and $\omega_{v\,n}^{D_2O}$ $(n = 1, 2, 3)$ may be evaluated by taking account of the mass difference between H and D:

$$\omega_{HR}^{D_2O} = \sqrt{\frac{1}{2}}\omega_{HR}^{H_2O} \quad \text{and} \quad \omega_{v\,n}^{D_2O} = \sqrt{\frac{1}{2}}\omega_{v\,n}^{H_2O}. \tag{8}$$

- It is assumed that the weights $\varepsilon_{t\,m}(T)$, $\varepsilon_{HR}^{D}(T)$ and $\varepsilon_{v\,n}$ for each vibrational mode are the same with those of liquid H_2O, together with their temperature dependence.

All the model parameters of liquid D_2O thus determined are listed in Table 1, whose values may be comparable with those of liquid H_2O [1].

3. Scattering properties of liquid D_2O

3.1. Generalized frequency distribution

The GFD as a function of $\hbar\omega$ is shown in Fig. 1 and compared with the result of molecular dynamics simulation [12], in which two components for D and O atoms are presented for $\hbar\omega$ up to 400 meV. There are four peaks in the component of D at about 5, 40, 150 and 340 meV, which arise from, respectively, the intermolecular vibration, the hindered rotation, the bending and stretching modes of intramolecular vibration. For the component of O, the translational motion of the molecule is dominant, though the simulation's result indicates appreciable contribution of the hindered rotation. As a result, it may be said that the present GFD is consistent with the one of molecular dynamics [12].

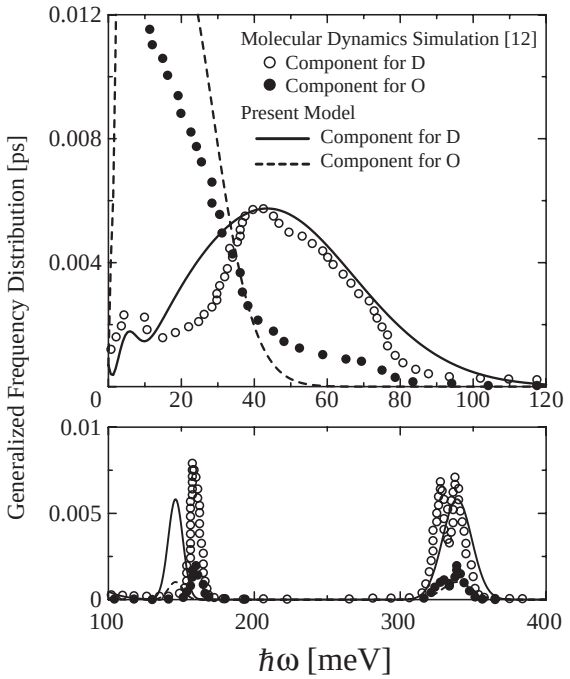

Fig. 1. GFD of liquid D_2O at 20 °C in terms of two components for D and O atoms, as compared with the molecular dynamics simulation [12].

3.2. Double-differential scattering cross section

Fig. 2 depicts the DDXs of liquid D_2O at 26 °C for $E = 213$ meV and scattering angle $\theta = 30°$, $60°$, $75°$ and $90°$. Also shown are the results of the neutron scattering experiment [5]. The calculated results are convoluted with a Gaussian resolution function having the half-

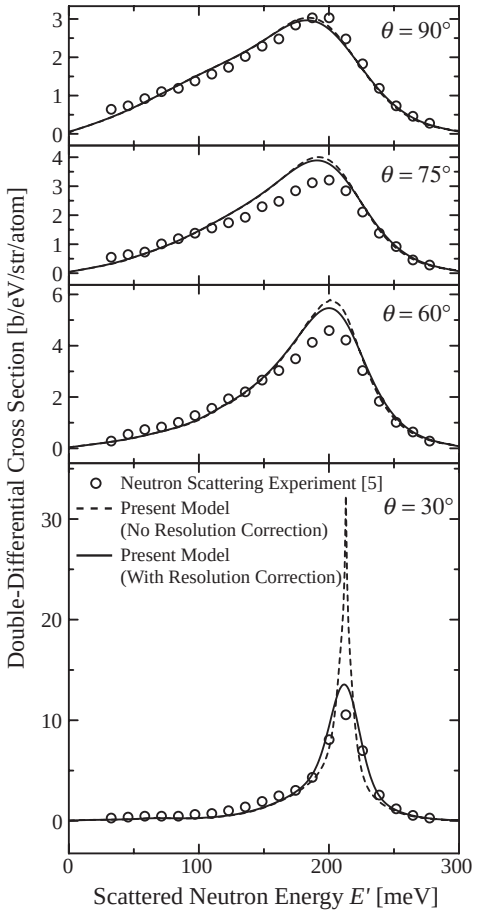

Fig. 2. DDXs of liquid D_2O at 26 °C for $E = 213$ meV and $\theta = 30°$, 60°, 75° and 90°: the experimental results by Harling [5] and the present model with and without the energy resolution correction.

width at half-maximum (HWHM) $\Delta E/E = 10\%$. The present model agrees with the experiment especially in terms of the following features: a quasi-elastic peak around $E' = 213$ meV, down (energy-loss) scattering due to the excitations of intermolecular vibrations and hindered rotation, and a slight peak at $E' = 70$ meV by the bending mode of intramolecular vibration. It may be noted that, compared with the DDXs for liquid H_2O [1], the present ones indicate a significant quasi-elastic component on account of the heavier mass of D_2O.

3.3. Scattering law

The scattering law $S^{D_2O}(Q,\omega)$ of liquid D_2O may be defined as

$$\left(\frac{d^2\sigma}{d\Omega\, dE'}\right)^{D_2O} = \frac{\sigma_b^{D_2O}}{4\pi k_B T}\sqrt{\frac{E'}{E}}S^{D_2O}(Q,\omega) \tag{9}$$

where

$$\sigma_b^{D_2O} = 2\left(4\pi {b_{coh}^{D}}^2 + 4\pi {b_{inc}^{D}}^2\right) + 4\pi {b_{coh}^{O}}^2 + 4\pi {b_{inc}^{O}}^2. \tag{10}$$

The quasi-elastic component of $S^{D_2O}(Q,\omega)$ is calculated for Q ranging from 0 to 2.5 Å^{-1} and characterized in terms of the HWHM. The results at 2 and 23 °C are shown in Fig. 3 as a function of Q^2, together with those by the cold neutron scattering experiment [6]. The static structure factor $S(Q)$ of liquid D_2O at room temperature

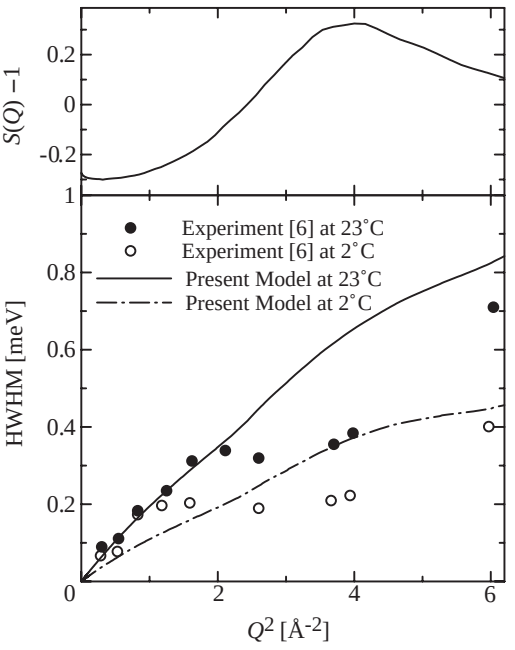

Fig. 3. HWHMs of liquid D_2O at 2 and 23 °C and the molecular structure factor $S(Q)$ defined by Eq. (12), together with the results of the neutron scattering experiment by Blanckenhagen [6].

is also shown in Fig. 3, defined by

$$S(Q) = \frac{4{b_{\mathrm{coh}}^{\mathrm{D}}}^2 S^{\mathrm{DD}}(Q) + 4b_{\mathrm{coh}}^{\mathrm{D}} b_{\mathrm{coh}}^{\mathrm{O}} S^{\mathrm{DO}}(Q) + {b_{\mathrm{coh}}^{\mathrm{O}}}^2 S^{\mathrm{OO}}(Q)}{4{b_{\mathrm{coh}}^{\mathrm{D}}}^2 + 4b_{\mathrm{coh}}^{\mathrm{D}} b_{\mathrm{coh}}^{\mathrm{O}} + {b_{\mathrm{coh}}^{\mathrm{O}}}^2} \tag{11}$$

$$= 0.486 S^{\mathrm{DD}}(Q) + 0.422 S^{\mathrm{DO}}(Q) + 0.0920 S^{\mathrm{OO}}(Q). \tag{12}$$

The calculated HWHMs increase monotonically with Q^2, while the experimental ones indicate a narrowing HWHM around $Q^2 \sim 4\,\mathrm{\AA}^{-2}$. The latter is related to the behavior of the first peak of $S(Q)$. This means that the present Vineyard approximation is too simple to describe $S^{\mathrm{D_2O}}(Q,\omega)$, especially with respect to collective excitations in the liquid. Some improvement for the description of coherent scattering has been made on liquid argon [31] and liquid H_2 and D_2 [20].

4. Cross-section libraries of liquid H_2O and D_2O

As a result of the previous [1] and present studies, it may be concluded that cross-section models of liquid H_2O and D_2O have been successfully developed over the range of incident neutron energies from 0.1 μeV (ultra-cold) to 10 eV (epi-thermal) and water temperatures from 0 to 100 °C. Hence the models may serve for generation of an advanced neutron cross-section library which would be useful for many practical purposes in the fields of neutron science and nuclear engineering.

4.1. Scattering law

Two sets of scattering laws, $S^{\mathrm{H_2O}}(Q,\omega)$ and $S^{\mathrm{D_2O}}(Q,\omega)$, for liquid H_2O and D_2O at 27 °C are calculated. They are defined by Eq. (9) and

$$\left(\frac{\mathrm{d}^2\sigma}{\mathrm{d}\Omega\,\mathrm{d}E'}\right)^{\mathrm{H_2O}} = \frac{\sigma_{\mathrm{b}}^{\mathrm{H_2O}}}{4\pi k_{\mathrm{B}} T}\sqrt{\frac{E'}{E}} S^{\mathrm{H_2O}}(Q,\omega) \tag{13}$$

where

$$\sigma_{\mathrm{b}}^{\mathrm{H_2O}} = 2\left(4\pi {b_{\mathrm{coh}}^{\mathrm{H}}}^2 + 4\pi {b_{\mathrm{inc}}^{\mathrm{H}}}^2\right) + 4\pi {b_{\mathrm{coh}}^{\mathrm{O}}}^2 + 4\pi {b_{\mathrm{inc}}^{\mathrm{O}}}^2 \tag{14}$$

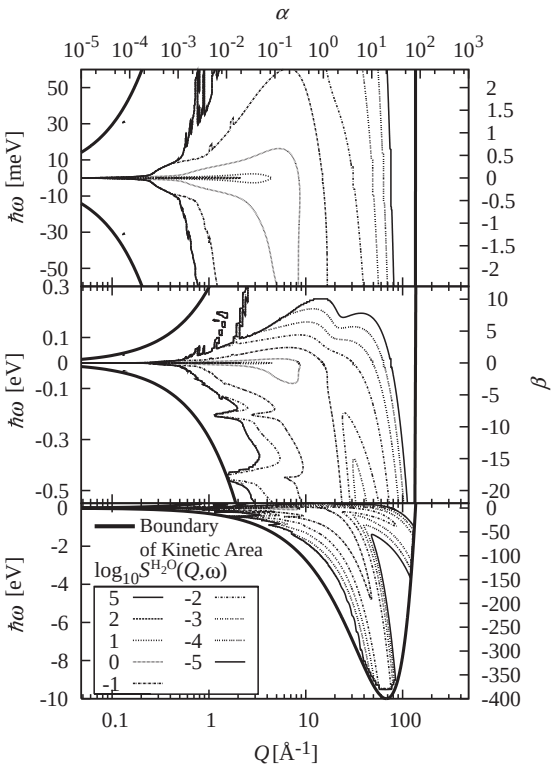

Fig. 4. Contour maps of the scattering law for liquid H_2O at 27 °C, by graphing $\log_{10} S^{\mathrm{H_2O}}(Q,\omega)$ in Q–ω space. The right and top axes express the dimensionless energy and momentum transfers defined by $\beta = \hbar\omega/k_{\mathrm{B}}T$ and $\alpha = (\hbar^2 Q^2/2m)/A_0 k_{\mathrm{B}} T$, respectively, where m is the neutron mass, $k_{\mathrm{B}}T = 25$ meV and $A_0 = 18$ as the mass number of H_2O.

and $S^{\mathrm{H_2O}}(Q,\omega)$ is the scattering law of liquid H_2O [1]. The results for liquid H_2O and D_2O are shown in Figs. 4 and 5, respectively, and are represented in the form of a contour map on the two-dimensional space of Q ($\mathrm{\AA}^{-1}$) and $\hbar\omega$ (meV). The conservation laws of energy and momentum for $E = 10$ eV are also plotted so that the areas of $S^{\mathrm{H_2O}}(Q,\omega)$ and $S^{\mathrm{D_2O}}(Q,\omega)$ on the Q–$\hbar\omega$ space are limited.

The whole scattering processes occurring over the range $Q = 0.01$–$100\,\mathrm{\AA}^{-1}$ and $\hbar\omega = -10$ eV–250 meV are graphically represented:

- quasi-elastic scattering around $\hbar\omega \sim 0$ meV for small Q,
- coherent effect on $S^{\mathrm{D_2O}}(Q,\omega)$ especially for $Q \sim 2\,\mathrm{\AA}^{-1}$ and $\hbar\omega \sim 0$ meV,

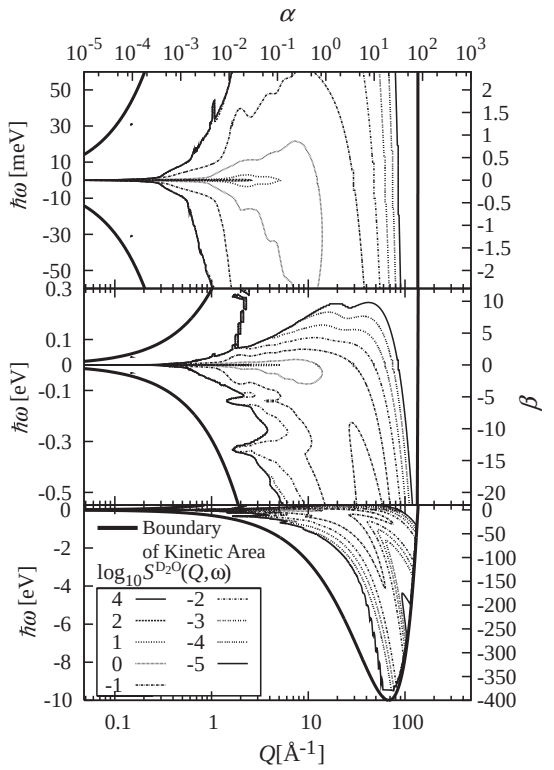

Fig. 5. Contour maps of the scattering law for liquid D_2O at 27 °C, by graphing $\log_{10} S^{D_2O}(Q,\omega)$ in Q–ω space. The right and top axes express the dimensionless energy and momentum transfers defined by $\beta = \hbar\omega/k_B T$ and $\alpha = (\hbar^2 Q^2/2m)/A_0 k_B T$, respectively, where m is the neutron mass, $k_B T = 25$ meV and $A_0 = 20$ as the mass number of D_2O.

- up- and down-scattering due to the existence of intermolecular vibration and hindered rotation in the range of $Q \sim 1$–$10\,\text{Å}^{-1}$ and $|\hbar\omega| \sim 5$–50 meV,
- down scattering by the excitation of intramolecular vibrations with $\hbar\omega \sim -210$ and -460 meV for H_2O and $\hbar\omega \sim -150$ and -340 meV for D_2O,
- recoil scattering in H, D and O for large energy transfer of $\hbar\omega < -1$ eV.

4.2. Multi-group constant

A set of multi-group constants (energy-averaged cross sections) for liquid H_2O and D_2O at 27 °C is generated (for the detailed definition, see Ref. [22]). The energy range from 0.1 μeV to 10 eV is divided at equal logarithmic intervals into $G = 80$ groups. The angular distribution of scattering cross section is represented by the Legendre expansion up to a maximum order $L = 3$, which is almost adequate for reproducing forward scattering in free H, D and O by an epi-thermal neutron. The weighting flux $\phi(E)$ is a Maxwellian plus $1/E$ spectrum with the same temperature as water. The group constant for liquid H_2O and D_2O is defined by

$$\sigma^{l,Y}_{s,g\to g'} = 2\pi \int_{-1}^{1} \mathrm{d}(\cos\theta)\, \sigma^{Y}_{s,g\to g'}(\theta) P_l(\cos\theta) \quad (15)$$

where

$$\sigma^{Y}_{s,g\to g'}(\theta) = \frac{1}{\int_{E_g}^{E_{g-1}} \mathrm{d}E\phi(E)} \times \int_{E_{g'}}^{E_{g'-1}} \mathrm{d}E' \int_{E_g}^{E_{g-1}} \mathrm{d}E\phi(E) \left(\frac{\mathrm{d}^2\sigma}{\mathrm{d}\Omega\,\mathrm{d}E'}\right)^{Y} \quad (16)$$

with $Y = H_2O$ or D_2O, $P_l(\cos\theta)$ is the Legendre polynomial function of order $l = 0, 1, 2, 3 (= L)$, and E_g and E_{g-1} are the lower and upper

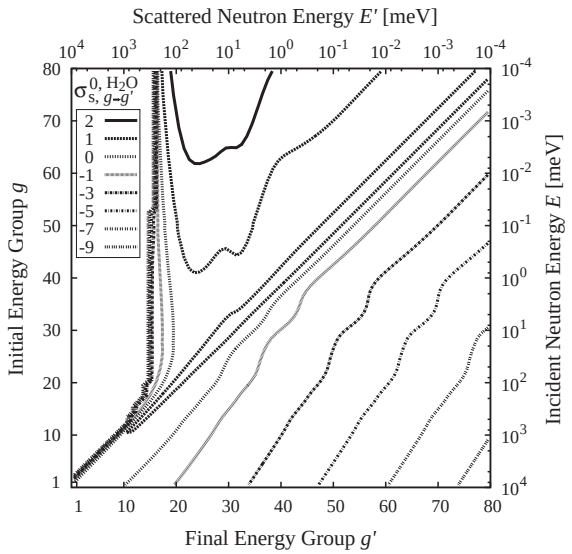

Fig. 6. Contour map of the transfer cross section $\sigma^{0,H_2O}_{s,g\to g'}$ for liquid H_2O at 27 °C. The right and top axes express the incident and scattered energies, E and E', respectively.

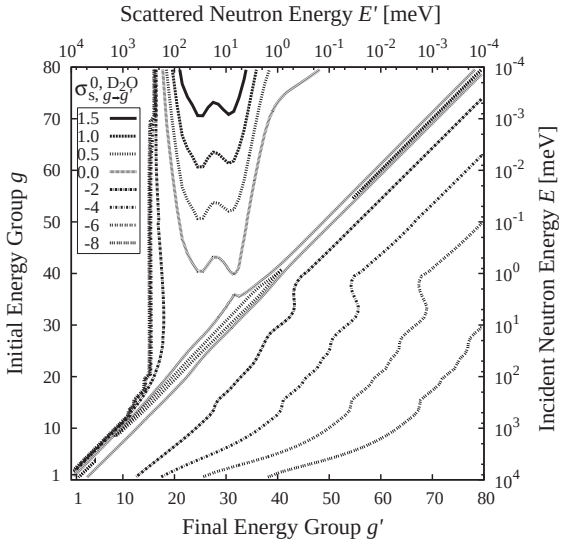

Fig. 7. Contour map of the transfer cross section $\sigma^{0,D_2O}_{s,g\to g'}$ for liquid D_2O at 27 °C. The right and top axes express the incident and scattered energies, E and E', respectively.

boundaries of the gth energy group ($g = 1, 2, 3, \ldots, G$).

Figs. 6 and 7 show the contour maps of $\sigma^{0,H_2O}_{s,g\to g'}$ and $\sigma^{0,D_2O}_{s,g\to g'}$, respectively, to illustrate neutron isotropic ($l = 0$) scattering associated with energy transfer from E (initial group g) to E' (final group g'). They are characterized by quasi-elastic scattering along $E \simeq E'$, down scattering for $E' < E$ and up scattering for $E < 0.1$ meV ($g > 50$) and $E' \sim 1$–100 meV ($20 < g' < 40$).

The angular distributions $f^Y_g(\theta)$ of scattered neutrons for an incident neutron of the gth energy group are shown in Fig. 8 for liquid H_2O and Fig. 9 for liquid D_2O, in which $f^Y_g(\theta)$ is obtained as

$$f^Y_g(\theta) = \sum_{g'=1}^{G} \sum_{l=0}^{L} \frac{2l+1}{4\pi} \sigma^{l,Y}_{s,g\to g'} P_l(\cos\theta). \qquad (17)$$

Liquid H_2O indicates forward scattering with increasing E above ~10 meV and an almost isotropic one for lower E. On the other hand, liquid D_2O exhibits an envelope line of coherent diffuse-Bragg scattering in the range of $1 < E < 20$ meV. This is indicated in terms of the Bragg-scattering condition $Q_{FP} = 2k \sin(\theta/2)$ under $Q_{FP} = 2\,\text{Å}^{-1}$ at which the first peak of $S(Q)$ is located (see Fig. 3).

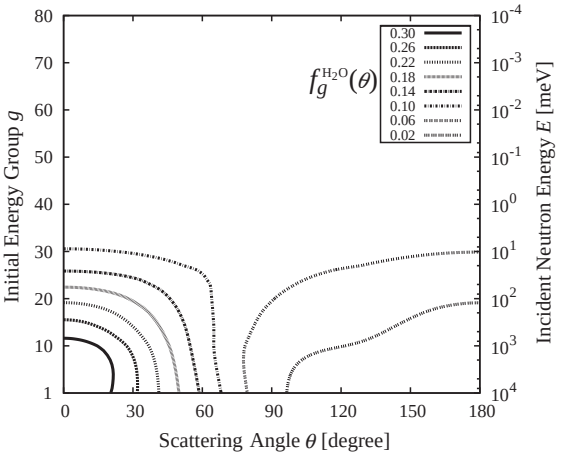

Fig. 8. Contour map of the angular distribution $f^{H_2O}_g(\theta)$ for liquid H_2O at 27 °C. The right axis expresses the incident neutron energy E.

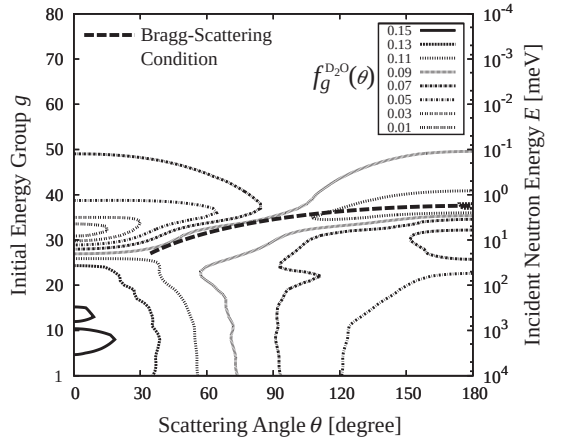

Fig. 9. Contour map of the angular distribution $f^{D_2O}_g(\theta)$ for liquid D_2O at 27 °C. The right axis expresses the incident neutron energy E.

Fig. 10 shows the total cross sections $\sigma^{H_2O}_t(g)$ and $\sigma^{D_2O}_t(g)$ and the total absorption cross section $\sigma^{H_2O}_a(g)$ for H_2O, together with the experimental values of BNL-325 [11]. Note that $\sigma^Y_t(g) = \sigma^Y_s(g) + \sigma^Y_a(g)$ and $\sigma^Y_s(g) = \sum_{g'=1}^{G} \sigma^{0,Y}_{s,g\to g'}$ though $\sigma^{D_2O}_a(g)$ is too small for the graphical presentation.

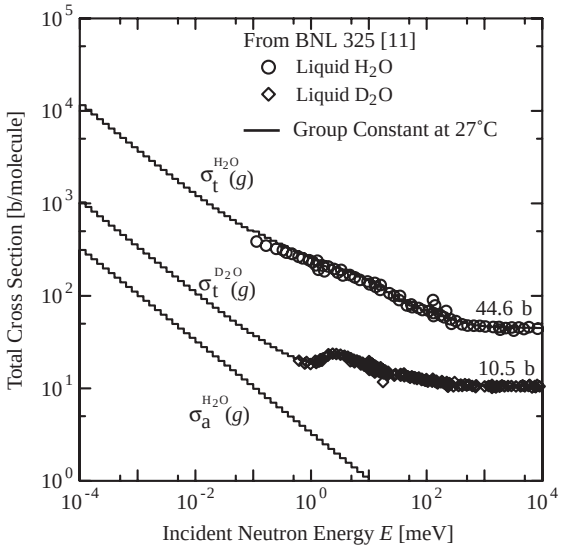

Fig. 10. Total cross sections of liquid H_2O and D_2O at 27 °C and the total absorption cross section of H_2O, together with the experimental results from BNL-325 [11].

The diffuse-Bragg scattering inherent in liquid D_2O is obvious around $E \sim 3$ meV and the transition of $\sigma_t^{H_2O}(g)$ and $\sigma_t^{D_2O}(g)$ to respective free atom cross sections is observed for $E > 1$ eV.

5. Concluding remarks

The double differential cross-section models for cold and thermal neutron scattering in liquid H_2O and D_2O are developed. The dynamics of molecules in the liquids is fully taken into account over the time range from 0.1 fs (a free-gas like behavior) to 1 μs (slow relaxation by diffusion). An effect of coherent scattering is also included simply by the Vineyard's convolution approximation. A variety of scattering results by experimental measurement and computer simulation are compared with the models, so that it is assured that the models are applicable to the wide range of neutron energies 0.1 μeV–10 eV and liquid temperatures 0–100 °C.

Two kinds of cross-section libraries for liquid H_2O and D_2O at room temperature are generated. The scattering laws will serve as a basic cross-section library in the fields of neutron science and nuclear technology: for instance, they may be useful for continuous-energy neutron transport (Monte Carlo) analysis and interpretation of neutron scattering results on various aqueous solution. The group-constant sets will be utilized for design and analysis of a neutron source and a nuclear reactor. By the combined use of the group constants for liquid ^4He, H_2, D_2, and CH_4 and solid CH_4 [20–25,32,33], it will be possible to proceed with the research and development of advanced pulsed and steady-state sources for ultra-cold, cold and thermal neutrons.

Acknowledgements

The authors are grateful to Dr. S. Tasaki who has made very valuable suggestions for developing the present cross-section models and libraries.

References

[1] Y. Edura, N. Morishima, Nucl. Instr. and Meth. A 534 (3) (2004) 531 URL http://dx.doi.org/10.1016/j.nima.2004.06.140.
[2] J. Teixeira, M.-C. Bellissent-Funel, S.H. Chen, A.J. Dianoux, Phys. Rev. A 31 (3) (1985) 1913.
[3] F. Cavatorta, A. Deriu, D.D. Cola, H.D. Middendorf, J. Phys.: Condens. Matter 6 (23A) (1994) A113.
[4] G.C. Lie, E. Clementi, Phys. Rev. A 33 (4) (1986) 2679.
[5] O.K. Harling, J. Chem. Phys. 50 (12) (1969) 5279.
[6] P.V. Blanckenhagen, Ber. Bunsenges. Phys. Chem. 76 (9) (1972) 891.
[7] M.-C. Bellissent-Funel, S.H. Chen, J.-M. Zanotti, Phys. Rev. E 51 (5) (1995) 4558.
[8] M. Sakamoto, B.N. Brockhouse, R.G. Johnson, N.K. Pope, J. Phys. Soc. Japan 17 (Suppl. B-II) (1962) 370.
[9] J.R. Beyster, Nucl. Sci. Eng. 31 (1968) 254.
[10] V.H.-D. Lemmel, Nukleonik 7 (1965) 265.
[11] D.I. Garber, R.R. Kinsey, Neutron cross sections BNL-325, vol. II, Curves, Technical report BNL-325, Brookhaven National Laboratory, 1976.
[12] G. Corongiu, E. Clementi, J. Chem. Phys. 98 (6) (1993) 4984.
[13] G.H. Vineyard, Phys. Rev. 110 (5) (1958) 999.
[14] G. Palinkas, E. Kalman, P. Kovacs, Mol. Phys. 34 (1977) 525.
[15] M. Nelkin, Phys. Rev. 119 (2) (1960) 741.
[16] H.C. Honeck, Trans. Am. Nucl. Soc. 5 (1962) 47.
[17] R.E. MacFarlane, New thermal neutron scattering files for ENDF/B-VI release 2, Technical report LA-12639-MS (ENDF-356), Los Alamos National Laboratory, Los Alamos, Oak Ridge, NM, 1994.

[18] V. McLane, ENDF-102 data formats and procedures for the evaluated nuclear data file ENDF-6, Technical report BNL-NCS-44945-01/04-Rev., National Nuclear Data Center, Brookhaven National Laboratory, Upton, NY, 2001.
[19] N. Morishima, D. Mizobuchi, Nucl. Instr. and Meth. A 350 (1) (1994) 275.
[20] N. Morishima, Y. Nishikawa, T. Mitsuyasu, Physica B: Condens. Matter 350 (Suppl. 1,1–3) (2004) E679.
[21] N. Morishima, Y. Sakurai, Nucl. Instr. and Meth. A 490 (3) (2002) 527.
[22] Y. Sakurai, T. Mitsuyasu, N. Morishima, Nucl. Instr. Meth. A 506 (1–2) (2003) 199.
[23] N. Morishima, Y. Matsuo, Nucl. Instr. and Meth. A 490 (1–2) (2002) 308.
[24] Y. Matsuo, N. Morishima, Y. Nagaya, Nucl. Instr. and Meth. A 496 (2–3) (2003) 446.
[25] N. Morishima, T. Mitsuyasu, Nucl. Instr. and Meth. A 517 (1–3) (2004) 295.
[26] F.J. Bermejo, M. Alvarez, S.M. Bennington, R. Vallauri, Phys. Rev. E 51 (3) (1995) 2250.
[27] F. Sacchetti, J.B. Suck, C. Petrillo, B. Dorner, Phys. Rev. E 69 (6) (2004) 061203 URL http://link.aps.org/abstract/PRE/v69/e061203.
[28] R. Mills, J. Phys. Chem. 77 (5) (1973) 685.
[29] D.J. Wilbur, T. DeFries, J. Jonas, J. Chem. Phys. 65 (5) (1976) 1783.
[30] T. DeFries, J. Jonas, J. Chem. Phys. 66 (12) (1977) 5393.
[31] K. Sköld, Phys. Rev. Lett. 19 (18) (1967) 1023.
[32] Y. Abe, N. Morishima, Nucl. Instr. and Meth. A 459 (1–2) (2001) 256.
[33] Y. Abe, N. Morishima, Nucl. Instr. Meth. A 481 (1–3) (2002) 414.